Research Article | Vol. 30, No. 3 / 31 Jan 2022 / Optics Express 4631

Optics EXPRESS

Quantum cascade laser absorption spectrometer with a low temperature multipass cell for precision clumped CO_2 measurement

AKSHAY NATARAJ,[1,2,*] MICHELE GIANELLA,[1] IVAN PROKHOROV,[1] BÉLA TUZSON,[1] MATHIEU BERTRAND,[2] JOACHIM MOHN,[1] JÉRÔME FAIST,[2] AND LUKAS EMMENEGGER[1]

[1] *Empa, Laboratory for Air Pollution / Environmental Technology, Dübendorf 8600, Switzerland*
[2] *ETH Zurich, Institute for Quantum Electronics, 8093 Zurich, Switzerland*
[*] *akshay.nataraj@empa.ch*

Abstract: We present a quantum cascade laser-based absorption spectrometer deploying a compact (145 mL volume) segmented circular multipass cell (SC-MPC) with 6 m optical path length. This SC-MPC is embedded into an effective cooling system to facilitate operation at cryogenic temperatures. For CO_2, the sample is cooled to 153 K, i.e. close to the sublimation point at 10 mbar. This enables efficient suppression of interfering hot-band transitions of the more abundant isotopic species and thereby enhances analytical precision. As a demonstration, the amount fractions of all three CO_2 isotopologues involved in the kinetic isotope exchange reaction of $^{12}C^{16}O_2 + {}^{12}C^{18}O_2 \rightleftharpoons 2\cdot{}^{12}C^{16}O^{18}O$ are measured. The precision in the ratios $[^{12}C^{18}O_2]/[^{12}C^{16}O_2]$ and $[^{12}C^{16}O^{18}O]/[^{12}C^{16}O_2]$ is 0.05 ‰ with 25 s integration time. In addition, we determine the variation of the equilibrium constant, K, of the above exchange reaction for carbon-dioxide samples equilibrated at 300 K and 1273 K, respectively.

1. Introduction

Accurate and precise measurements of multiply-substituted ("clumped") isotopologues of carbon dioxide have become an exciting new tool in the fields of biogeochemistry, paleoclimate research [1,2], atmospheric sciences, and other fields of environmental research. One important aspect of this approach is that the analysis of multiply-substituted isotopologues can directly provide temperatures for the investigated system through the thermodynamically determined abundance. The basis for it lies in the temperature dependence of the equilibrium constant K(T) of the isotope exchange reactions $^{12}C^{16}O_2 + {}^{13}C^{16}O^{18}O \rightleftharpoons {}^{13}C^{16}O_2 + {}^{12}C^{16}O^{18}O$ and $^{12}C^{18}O_2 + {}^{12}C^{16}O_2 \rightleftharpoons 2\cdot{}^{12}C^{16}O^{18}O$, respectively [3]. Since the isotopologue abundance in such a homogeneous isotope exchange reaction is only set by thermodynamics, it unambiguously provides temperature information under equilibrium conditions and no further assumptions are needed. As such, unlike the standard oxygen paleothermometry, clumped isotope thermometry is independent of the oxygen isotopic composition of the solution from which the carbonates are formed [4–7].

Currently, the established method to perform clumped isotope thermometry is Isotope Ratio Mass Spectrometry (IRMS) [8,9]. However, IRMS measurements, in particular for rare isotopologues, typically require several hours of analysis time and extensive sample preparation to properly separate isobaric interferences. Moreover, several CO_2 isotopologues have the same cardinal mass (e.g. $^{12}C^{18}O^{17}O$ and $^{13}C^{16}O^{18}O$ of 47 amu, $^{13}C^{18}O^{17}O$ and $^{12}C^{18}O_2$ of 48 amu), which requires very high mass resolution or assumption-based correction schemes [10].

In contrast to IRMS, optical absorption spectroscopic techniques allow the realisation of isotopologue specific, non-destructive, and compact spectrometers with short analysis time and high-precision capabilities. Recently, Wang et al. [11] and Prokhorov et al. [12] have

#447172 https://doi.org/10.1364/OE.447172
Journal © 2022 Received 3 Nov 2021; revised 10 Dec 2021; accepted 10 Dec 2021; published 28 Jan 2022

Optics EXPRESS

demonstrated the great promise of laser absorption spectroscopy for measurements of clumped isotopes of carbon dioxide.

The major challenge for clumped isotope thermometry of $^{12}C^{18}O_2$ resides in its very low natural relative abundance (4.1 ppm) and the omnipresent spectral interference from the main (CO_2) and its other abundant isotopic species, e.g. singly-substituted isotopologues. These factors seriously limit the achievable analytical performance of spectroscopic measurements and thus the applicability of this technique. The precision of spectroscopic measurements involving isotopic species that are hidden by the hot-band transitions of the more abundant isotopes can be, however, improved under low-temperature and low-pressure conditions. The interference caused by the hot-band transitions of the main isotopic species can be suppressed at low temperatures and the absorption line width is narrower at low pressures. This is especially the case when measuring rare species like $^{14}CO_2$ [13,14] or clumped isotopes.

In this paper, we address this challenge by using a quantum cascade laser absorption spectrometer (QCLAS) employing a low-volume segmented circular multipass cell (SC-MPC) that can be operated at cryogenic temperatures. This approach aims to reduce the spectral interferences from the hot-band transitions of more abundant isotopologues and can be applied to other molecular species that cannot be measured under room temperature conditions with sufficient accuracy.

The setup allows simultaneous and high precision measurement of all the three isotopologues of CO_2 involved in the isotope exchange reaction between $^{12}C^{18}O_2$ and $^{12}C^{16}O_2$. To demonstrate the performance of the spectrometer, we also measure the change in equilibrium constant, K(T), of the isotope exchange reaction between pure CO_2 samples equilibrated at two distinct temperatures, i.e. at 300 K and 1273 K, respectively.

2. Method

Applying laser spectroscopy as clumped isotope thermometry, one has to determine the subtle changes in the equilibrium constant K value, which then reflect the temperature during equilibration/formation. This involves the simultaneous and unambiguous measurement of all isotopic species involved in the isotope exchange reaction. For example, the isotope exchange reaction

$$^{12}C^{16}O_2 + {}^{12}C^{18}O_2 \overset{K(T)}{\rightleftharpoons} 2 \cdot {}^{12}C^{16}O^{18}O \tag{1}$$

where the temperature-dependent equilibrium constant K(T) is defined as

$$K(T) = \frac{[^{12}C^{16}O^{18}O]^2}{[^{12}C^{16}O_2][^{12}C^{18}O_2]}, \tag{2}$$

involves the amount fractions of isotopologues $^{12}C^{16}O_2$, $^{12}C^{18}O_2$ and $^{12}C^{16}O^{18}O$.

Measuring accurate values for the amount fractions of the three isotopologues is, however, challenging due to: i) instrumental biases (absolute values of the absorption path length, gas temperature and pressure), ii) uncertainties of the spectroscopic parameters (line strength, collisional broadening parameter), and iii) systematic errors arising from spectral fitting. We overcome this problem by normalizing amount fractions, [X], of a sample gas with the corresponding amount fraction measured in a reference gas, $[X]_{ref}$. This removes any systematic errors common to both the sample and reference measurements. Therefore, we consider the ratio

$$\frac{K(T)}{K(T_{ref})} = \frac{\left([^{12}C^{16}O^{18}O]/[^{12}C^{16}O^{18}O]_{ref}\right)^2}{\left([^{12}C^{16}O_2]/[^{12}C^{16}O_2]_{ref}\right)\left([^{12}C^{18}O_2]/[^{12}C^{18}O_2]_{ref}\right)} \tag{3}$$

or its logarithm

$$\kappa(T, T_{ref}) = -\ln \frac{K(T)}{K(T_{ref})}. \tag{4}$$

Optics EXPRESS

because the deviation of K(T) from $K(T_{ref})$ is typically very small. Usually, the reference material is related to the stochastic distribution, calculated from the bulk isotopic composition [15]. In practice, this is achieved using gas samples equilibrated at high temperatures, where the atoms reach stochasticity among the molecules. The equilibrium constant in the high-temperature (stochastic) limit is indicated by K^*. The deviation of K(T) from K^* is given by the quantity Δ(T), defined as [15]

$$\Delta(T) = -\ln \frac{K(T)}{K^*}. \tag{5}$$

From Eqs. (4) and (5) we derive

$$\kappa(T, T_{ref}) = \Delta(T) - \Delta(T_{ref}). \tag{6}$$

There are several theoretical calculations of the temperature dependence of Δ available (see e.g. [16] and references therein). Based on these values, the expected difference in Δ(T) between room- and high-temperature case can be estimated to −0.345 ‰.

In terms of spectroscopy, the most promising spectral range for measuring the isotopologues $^{12}C^{18}O_2$,$^{12}C^{16}O^{18}O$ and $^{12}C^{16}O_2$ is in the 4.3 µm range, where the CO_2 has its fundamental asymmetric stretching mode (ν_3). Prokhorov et al. [12] proposed the spectral window around 2305 cm^{-1}, where the absorption lines of the isotopologues are relatively well isolated from other potential interfering species. The absorption lines used in this study are listed in Table 1.

Table 1. List of absorption lines selected for this study. The spectroscopic parameters were taken from the HITRAN database [17,18]: ν is the center frequency of the transition, S(296) and S(153) are the abundance-weighted line strengths of the transition at 296 K and 153 K, respectively, E'' is the energy of the lower state of the transition, v' and v'' are the upper- and lower-state vibrational quantum numbers, and Br(J'') is the branch symbol and the lower-state rotational quantum number.

Isotopologue	ν (cm^{-1})	S(296) (10^{-23} cm^2cm^{-1}/molecule)	S(153)	E'' (cm^{-1})	$v' \leftarrow v''$	Br(J'')
$^{12}C^{18}O_2$	2305.3654	1.11	1.82	54.1	$(00^01) \leftarrow (00^00)$	P(12)
$^{12}C^{16}O_2$	2305.5134	432	0.848	1533	$(02^21) \leftarrow (02^20)$	P(22)
$^{12}C^{16}O^{18}O$	2305.5679	24.9	1.55	788	$(01^11) \leftarrow (01^10)$	P(18)

However, at room temperature, the challenge to measure $^{12}C^{18}O_2$ is due to the spectral interference from the main $^{12}C^{16}O_2$ isotopologue. The situation is illustrated in Fig. 1(a) that shows the transmission spectra of pure CO_2 at 5.3 mbar pressure measured at two distinct temperatures: 296 K and 153 K, respectively. Reducing the gas temperature de-populates the rotational levels of the hot-band transitions, thereby lowering their intensity and hence their disturbing contribution. Cooling the sample gas to 153 K, the line strength of the main isotopologue is suppressed by almost three orders of magnitude. In contrary, the absorption of $^{12}C^{18}O_2$ even increases slightly, because it is a ground state transition with relatively low J value, benefiting from the thermal distribution of the rotational levels at lower temperatures. The most pronounced effect is observed for the weaker absorption line of $^{12}C^{18}O^{17}O$ at 2305.43 cm^{-1}, which, at room temperature, is completely hidden under the strong hot-band transition of $^{12}C^{16}O_2$. In short, lowering the gas temperature, is beneficial for distinguishing adjacent spectral lines more efficiently, thereby enhancing the specificity and precision of the technique. Figure 1(b), shows the measured temperature dependence of the line strengths associated to $^{12}C^{18}O_2$ and $^{12}C^{16}O^{18}O$ transitions along with the corresponding standard deviation. Comparing these results with the theoretical dependencies calculated from the molecular parameters, we found a good agreement, especially for the $^{12}C^{18}O_2$ isotopologue. However, for the $^{12}C^{16}O^{18}O$ species, there is an increased discrepancy between the measured and theoretical values towards higher temperatures. The reason for this mismatch remains unresolved and definitely requires more

Optics EXPRESS

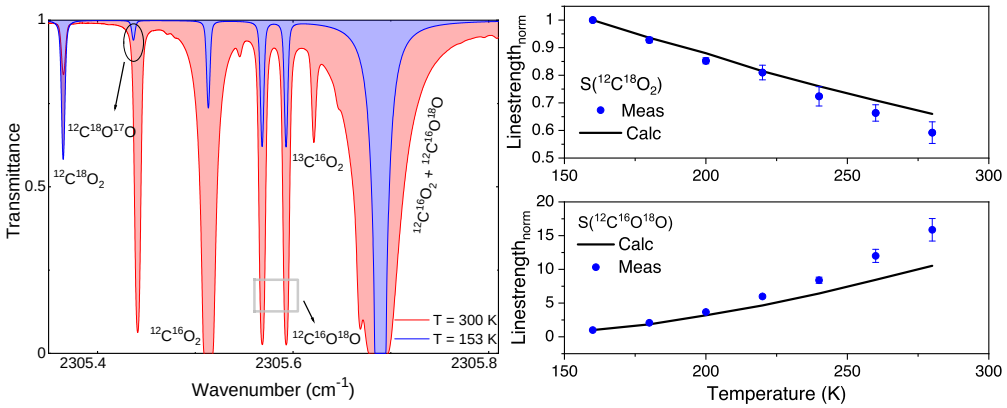

(a) (b)

Fig. 1. (a) Measured transmission spectra of natural pure CO_2 recorded at 300 K (red trace) and 153 K (blue trace) using the SC-MPC with 6 m optical path length at a gas pressure of 5.3 mbar. The individual isotopic species are marked. (b) Temperature dependency of the measured line strengths (blue dots) of $^{12}C^{18}O_2$ (top) and $^{12}C^{16}O^{18}O$ (bottom), normalized to 160 K, along with the calculated behavior based on the parameters from HITRAN database [17].

investigation. However, it should be recognized that with increasing temperature the absorption lines are getting saturated, which makes accurate fitting more difficult. This may introduce a bias in our measured values.

The above aspects were fully considered in the design and development of the laser spectrometer. A schematic drawing of the experimental setup is shown in Fig. 2(a). The spectral range around 4.3 µm was accessed by using a thermo-electrically cooled distributed feedback quantum cascade laser (DFB-QCL) operated in intermittent Continuous Wave (iCW) mode [19]. The emission frequency of the laser is scanned over 1 cm^{-1} range at a repetition rate of 6.5 kHz using a custom-made laser driver [20]. A plano-convex lens of focal length 250 mm is used to couple the beam into a 145 mL-volume SC-MPC with an effective optical path length of 6 m [21]. The output beam is focused onto a MCT photodetector (PVM-2TE-10.6, VIGO System) using an off-axis parabolic mirror. A wedged neutral density (ND) filter close to the laser housing is used to: i) attenuate the optical power, thus avoiding detector saturation, and ii) to reduce optical feedbacks that impact optical fringe level. The relative frequency scale of the laser scan is obtained by using a secondary optical path with a Germanium étalon with a free spectral range of 720 MHz inserted in the beam path.

The SC-MPC used in this setup was developed by Graf et al. [21]. It consists of an aluminium ring with inner diameter of 108.82 mm with 57 mirror segments carved into the inner surface. This special monolithic design makes the SC-MPC robust and resistant to thermal distortions as demonstrated in recent field applications [22,23] and, therefore, fully suitable for the targeted low-temperature measurements as presented in this study.

The multipass cell is sealed by two 8 mm-thick gold-plated circular copper discs. Gas inlets are mounted to the upper lid. Indium wire was used instead of rubber O-rings to achieve a gas-tight seal even under cryogenic temperatures. The SC-MPC is mounted inside a custom-made vacuum chamber (Fig. 2(b)). The stainless-steel vacuum chamber is cylindrical with an inner diameter of 261 mm and an inner height of 132 mm. It features two ISO-K 250 flanges that fit two circular aluminium lids, as well as 8 radially arranged flanges: (i) two ConFlat 2.75-inch outer diameter flanges for the two BaF_2 optical windows (Thorlabs); (ii) one ISO-K 63 flange

Optics EXPRESS

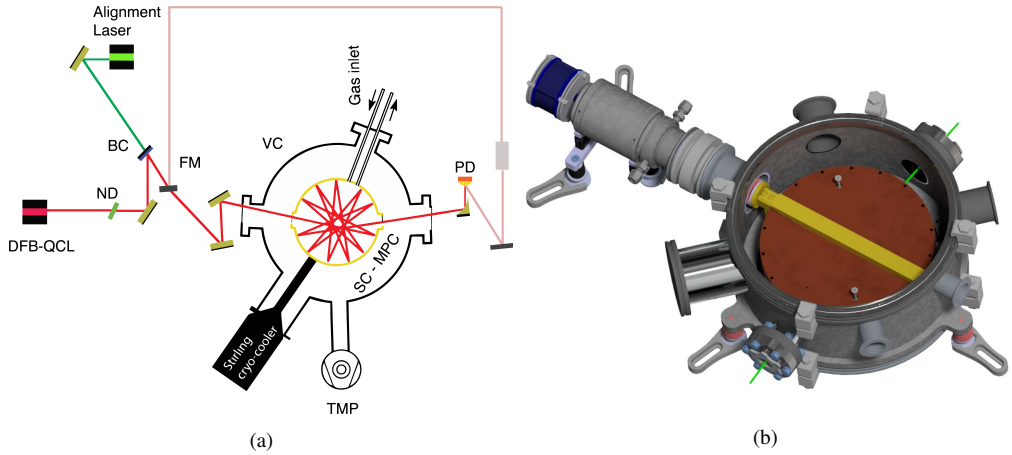

Fig. 2. (a) Schematic drawing of the experimental QCLAS setup. ND: neutral density filter, BC: IR/VIS beam combiner, FM: flip mirror, VC: vacuum chamber, PD: photodetector, TMP: turbo-molecular pump. The trace laser is used to facilitate aligning the DFB-QCL into the SC-MPC. (b) 3D drawing of the vacuum chamber with the SC-MPC inserted.

for the vacuum pump (HiCube 80, Pfeiffer Vacuum); (iii) one QF 50 flange for the Stirling cooler (MT11904001AA, Sunpower-Ametek); (iv) two QF 40 flanges for connecting the Pt100 sensor required by the temperature control loop of the Stirling-cooler and for the pressure gauge (PKR 251, Pfeiffer Vacuum); and (v) two QF 25 flanges for the gas and thermocouple feedthroughs. The turbo-molecular pump is used to maintain the chamber pressure at 2×10^{-5} mbar. This evacuated volume represents a very efficient thermal decoupling from the ambient, allowing the SC-MPC to be cooled to cryogenic temperatures, while avoiding condensation of water on the cold SC-MPC windows. The cell pressure is monitored by a piezo/pirani combination manometer (CMR 363, Pfeiffer Vacuum) and regulated with a pressure regulator (PC-series, Alicat).

The SC-MPC is cooled down to 153 K using the Stirling cooler. A copper bar acts as a thermal bridge between the cold tip of the Stirling cooler and the top and bottom lids of the SC-MPC. The temperature of the cold tip is continuously monitored using a Pt100 sensor and serves as input to the PID controller that maintains the set temperature within 5 mK. Two additional thermocouples are attached at different points on the upper lid of the SC-MPC to obtain further temperature readings.

As ambient temperature fluctuation have negative impact on the long-term performance of the spectrometer, the entire setup is covered with an acrylic-glass housing. The temperature within the enclosure is further stabilised using an air-to-air thermo-electric cooler (AA-150-24-22-00-00, Laird Thermal Systems). Furthermore, the enclosure is purged with CO_2-free air (MCA621, Altec Air) at 20 L min^{-1} to avoid ambient CO_2 absorption along the free-space optical path.

An automatic gas handling system based on a multi-port valve with a micro-electric actuator (EUTA11937, VICI) allows rapid switching between sample and reference gas. In our case, the reference gas is pure CO_2 (purity 4.5, 10 L, PanGas AG). The gas line is made out of 1/16 inch stainless-steel tubing and works in a flow-through mode, wherein a combination of a needle valve at the output of the cell and a pressure regulator at the inlet is used to maintain the pressure inside the MPC at 5.3 mbar with a flow rate of 1 mL min^{-1}. A membrane pump (KNF Neuberger AG) is used to continuously draw gas through the SC-MPC. For the repeatability characterisation (see Sect. 3.1), a measurement cycle was defined, where each sample measurement is bracketed by two working reference measurements, each step lasting for 200 s. This allowed for instrument drift correction along a sequence of sample analysis. The hardware control and data acquisition

Optics EXPRESS

system were developed in-house (for details see [20,23]) using an integrated System-on-Chip (Red Pitaya [24]) solution.

In addition to the above described system, a peripheral setup was realized that allowed for in-house generation of the high-temperature CO_2 samples. Thus, gas samples (n = 5) were prepared in quartz tubes using pure CO_2 from a pressurized gas cylinder. The tubes were pre-treated by baking them in an oven at 100 °C for 5 h and evacuating them down to 1×10^{-6} mbar. Afterwards, they were filled with 4.5 mmol of pure CO_2 and sealed by melting the glass tubing with a propane-oxygen torch. The sealed tubes were then heated in an oven at 1273 K ± 2 K for 8 h to assure re-equilibration. The carbon dioxide was extracted from the tubes using the following procedure: first the tubes were taken out from the oven and immersed in liquid N_2 to freeze out the carbon dioxide. Once attached to the purification line (see Fig. 3), the seal was mechanically broken under vacuum conditions (1×10^{-6} mbar), the glass tubes warmed up and their content introduced into the purification line for further removal of potential impurities of water and other non-condensable gases. This involved a two stage process, where potential contamination from water was removed at the first stage of the purification line by immersing the first trap in an ethanol bath at 243 K and trapping the sample CO_2 for 3 min. Afterwards, the sample was transferred to the liquid N_2 cooled second trap to freeze out the carbon dioxide and pump out the non-condensable impurities. The purified sample was collected into a 10 mL cylinder (SS-4CS-TW-10, Swagelok), which was then attached to the multi-port inlet of the gas handling system.

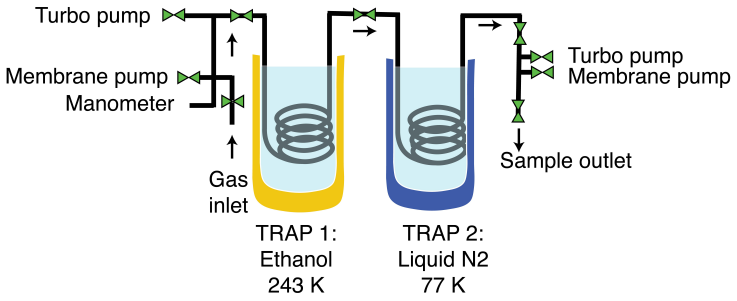

Fig. 3. Purification line used to extract the prepared CO_2 samples.

Prior to the high-temperature sample measurements, we investigated whether passage of the carbon dioxide samples through the purification line introduces any fractionation (a selective depletion/enrichment of an isotopologue relative to the others, leading to an unwanted change in the isotopologue ratio). Therefore, we transferred five samples taken from the gas cylinder through the purification line, applied the above described handling steps (e.g. trapping and pumping) and then compared their isotopologue ratios with the respective ratios measured on samples directly taken from the gas cylinder. The deviations of the ratios from the expected value of 1, were within the established precision of the spectrometer of 0.05 ‰ (see section 3.1).

Finally, it should be noted that in the process of high-temperature equilibration followed by purification, a systematic loss of about 0.7 % of the initial CO_2 has been observed. This raised the question, whether the concentration difference might have an impact on the determined relative isotope ratios and the calculated equilibrium constant. It is known that isotope ratios tend to show some degree of dependence on total amount fraction (e.g. [25]). In order to verify this, we diluted 200 mL of the reference gas CO_2 with 2 mL of N_2, resulting in a CO_2:N_2 mixture with 100:1 mixing ratio. These samples were then measured against the undiluted reference gas. The equilibrium constant showed a linear dependence of −0.01 ‰ for every 0.1 % increase in concentration. This bias was corrected in all consecutive determinations.

Optics EXPRESS

3. Results

3.1. Spectrometer performance

To determine the precision and sensitivity of the system, we first recorded the transmission spectrum of the empty cell, used for normalizing purposes, then filled the cooled SC-MPC with 5.3 mbar pure CO_2 and acquired a time series of 1000 s. An example of 1 s averaged transmission spectrum of pure CO_2 measured at low temperature (153 K) and pressure (5.3 mbar) in the SC-MPC is shown in Fig. 4. As mentioned above, single spectral scans are acquired in 160 µs, and thus co-adding 6250 scans results in a transmission spectrum every 1 s. These spectra are normalized either in-fly or in a post-processing step by the empty cell transmission, while the absorption lines (see Table 1) are fitted in real-time by a Voigt profile using Levenberg–Marquardt least-squares algorithm implemented in LabVIEW (National Instruments, USA). The baseline structure is described by a 3rd order polynomial, which is determined within the line fitting process, using segments of the spectra with no absorption. The achieved minimum detectable absorption (MDA) is 2.94×10^{-5}. This corresponds to a noise equivalent absorption sensitivity (NEAS) of $4.9 \times 10^{-8}\,\mathrm{cm^{-1}\,Hz^{-1/2}}$ [26]. The "w-shaped" residual seen in Fig. 4 is due to the unaccounted collisional narrowing and speed dependence of the relaxation rate, which is an inherent limitation of the Voigt profile [27,28]. This might lead to a systematic error in the measured abundances of the individual isotopologues [29]. To overcome this limitation, we measure *ratios* of amount fractions, while maintaining the same pressure and temperature conditions for both sample and reference measurements and thus we expect any such systematic error to cancel out. Considering Eq. (2), the equilibrium constant can also be expressed with the two isotopologue ratios,

$$R_1 = [^{12}C^{16}O^{18}O]/[^{12}C^{16}O_2], \tag{7}$$

and

$$R_2 = [^{12}C^{18}O_2]/[^{12}C^{16}O_2] \tag{8}$$

as

$$K(T) = \frac{R_1^2}{R_2}. \tag{9}$$

Figure 5(a) (top panel) shows the relative deviations of isotopologue ratios R_1, R_2 (Eqs. (7) and (8)) and K (Eq. (9)) from their respective means. In the bottom panel, we show the Allan-Werle

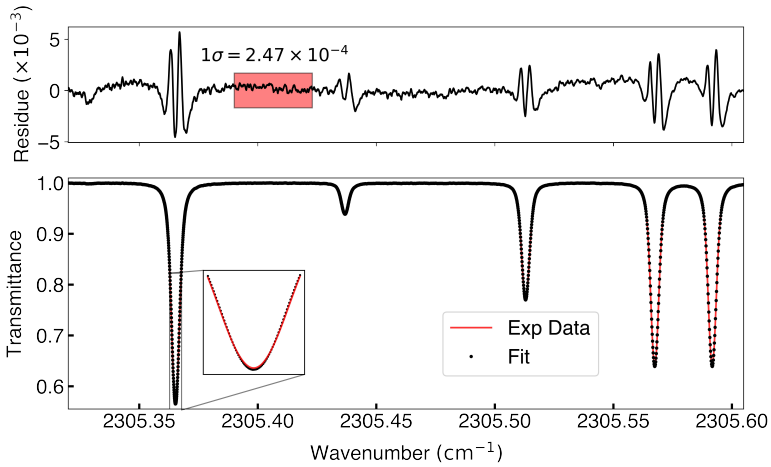

Fig. 4. Measured transmission spectrum of pure CO_2 at T = 153 K and p = 5.3 mbar with fitted Voigt lineshapes.

Optics EXPRESS

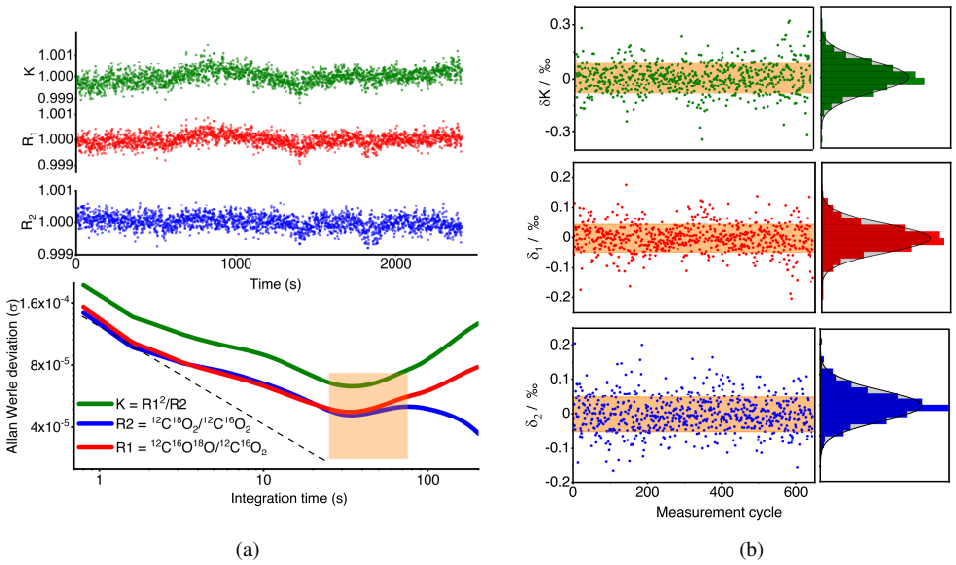

(a) (b)

Fig. 5. (a) Allan-Werle deviation as a function of integration time and the associated time series of the two absorption ratios and the equilibrium constant (K). The shaded region shows the typical integration time used in the study. (b) 72 h long measurement to demonstrate the repeatability of the instrument. Each data point corresponds to the relative change in the isotope ratio between two consecutive measurements.

plot associated to the three quantities above. The best achieved precision after 25 s integration time is 0.050 ‰ in R_1 and R_2 and 0.065 ‰ in K. On larger averaging time, the precision is impacted by thermal drifts and optical fringes.

The repeatability of the system was investigated by performing a series of 650 measurement cycles, where sample and reference were the same gas, i.e. alternating between the two inputs of the multi-port inlet attached to the same gas cylinder. For each measurement cycle, the first 175 s were discarded to avoid potential biases due to switching and incomplete purging, and only the last 25 s data segment was used to calculate the ratios R_1 and R_2, as well as the equilibrium constant K for both sample and reference case. Then we computed the relative deviation of the ratios, $\delta_i = R_{isampl}/R_{iref}$ where i = 1, 2 (see Eqs. (7) and (8)) and of the equilibrium constant:

$$\delta K = \frac{K_{sample}}{K_{ref}} - 1 = \frac{(1+\delta_1)^2}{1+\delta_2} - 1, \tag{10}$$

We expect δ_i and δK, to be zero on average as both the sample and reference gas originate from the same gas cylinder. In Fig. 5(b), we show these quantities for each of the 650 measurement cycles and their corresponding probability density functions (PDFs). The PDFs (in units of ‰) are calculated with 20 bins of width 0.025 ‰ for δ_1, δ_2 and 0.035 ‰ for δK. The standard deviations of δ_1, δ_2 and δK are 0.05 ‰, 0.047 ‰ and 0.083 ‰, respectively. These values are in accordance with the Allan-Werle deviation values found for the isotopologue ratios at 25 s integration time (Fig. 5(a)).

3.2. *Clumped isotope thermometry based on $^{12}C^{18}O_2$*

The applicability of the spectrometer for clumped isotope thermometry is best illustrated by measuring the relative change in the equilibrium constant value at two distinct formation temperatures. In this study we consider the room-temperature (300 K) and the high-temperature

Optics EXPRESS

(1273 K) cases only. The underlying assumption is that the reference CO_2 gas in the pressurized cylinder is well equilibrated at room-temperature due to two factors: i) the CO_2 originates from minerals (carbonates) formed most likely at ambient temperatures and ii) the gas was stored for long enough time such that it is equilibrated at this storage temperature. The high-temperature samples had to be prepared in-house. Therefore, we equilibrated five samples at T = 1273 K (see sect. 2.), and measured the value of the equilibrium constant, K(T), relative to the value obtained for the reference gas taken directly from the gas cylinder, i.e. with $K(T_{ref} = 300\,K)$. Each sample was analyzed six times using a measurement cycle similar to the repeatability experiments, i.e. bracketed with reference gas measurements, and measured for the duration of the stability range (20 s). These repeated measurements were averaged and used to determine κ (see Eq. (4)).

Figure 6 summarizes the averaged values of κ obtained for the five individual samples. The mean value $\bar{\kappa} = -0.34$ ‰ ± 0.02 ‰ is in very good agreement with the theoretical value of −0.345 ‰.

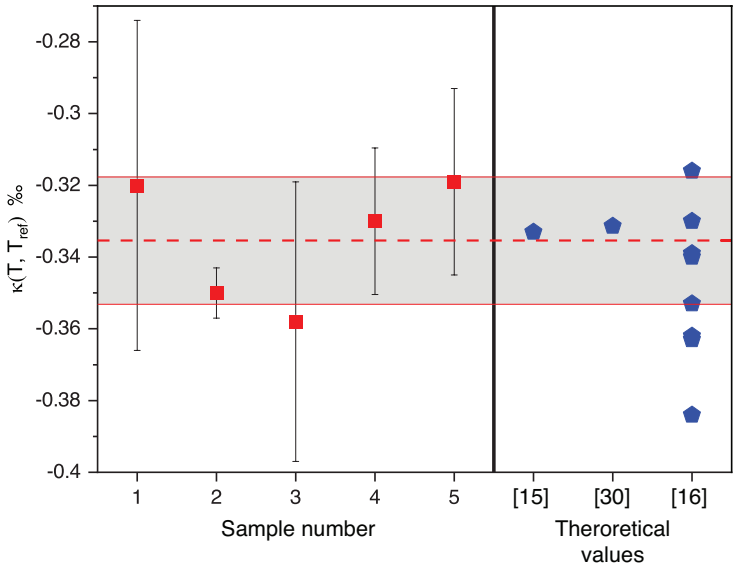

Fig. 6. Measured values of κ (Eq. (4)) from repeated equilibration experiments (red markers). The error bars indicate the individual precision of each measurement. The blue markers show the theoretical values from Wang et al. [15], Cerezo et al. [30] and Cao et al. [16].

Overall, the successful combination of low-volume cooled SC-MPC, low-noise laser driver and fast DAQ combined with well stabilized temperature and pressure control enabled us to detect and resolve the tiny variation in the equilibrium constant value of the isotope exchange reaction for CO_2 samples experiencing different temperatures. Similar quality has been previously demonstrated by only one other research group using IRMS [9]. The setup can be further extended by implementing a dual laser configuration to simultaneously measure $\Delta_{^{12}C^{18}O_2}$ and $\Delta_{^{13}C^{16}O^{18}O}$. This allows to interpret correlations of both parameters using dual-clumped-isotopologue plots and distinctively identify deviations from theoretical predictions, which signify non-equilibrium (e.g. kinetic) processes [31]. Furthermore, the concept can be applied for other isotopologues like $^{14}CO_2$ or molecular species, for example CH_2D_2 or C_3H_8 and its position specific isotopomers, which are excellent tracers for anthropogenic emissions [32–34].

Optics EXPRESS

4. Conclusion

A compact mid-infrared QCLAS spectrometer for measuring the clumped CO_2 isotopologues was realised, relying on a low-volume Stirling-cooled SC-MPC. The low-temperature approach was implemented to minimize spectral interferences and achieve high precision. This spectrometer was used for unambiguous detection of all isotopologues involved in the isotope exchange reaction of $^{12}C^{18}O_2 + {}^{12}C^{16}O_2 \rightleftharpoons 2 \cdot {}^{12}C^{16}O^{18}O$ with a precision of 0.05 ‰ on the measured isotope ratios, and 0.065 ‰ on the equilibrium constant. As a demonstration of its potential, we resolved relative changes in the temperature dependent equilibrium constant (K(T)) for CO_2 equilibrated at 1273 K and the reference gas at room temperature. This versatile system can be extended to rare isotopic species of other molecules, which are eventually seriously impacted by the hot band transitions of abundant isotope species, thereby opening up new perspectives in environmental sciences and fundamental research.

Funding. Schweizerischer Nationalfonds zur Förderung der Wissenschaftlichen Forschung (157208, 40B2-0_176584).

Acknowledgement. The authors gratefully acknowledge Herbert Looser, André Kupferschmid, and Philipp Scheidegger for their software and hardware development as well Manuel Graf for the development of SC-MPC. Further, many thanks to Mattias Beck and Filippos Kapsalidis for processing the laser. We would also like to thank Erwin Pieper and Erich Heiniger from the mechanical engineering workshop at Empa for their support and helpful discussions related to MPC design and vacuum chamber realization.

Disclosures. The authors declare no conflicts of interest.

Data availability. Data underlying the results presented in this paper are available in Ref. [35].

References

1. J. M. Eiler, "Paleoclimate reconstruction using carbonate clumped isotope thermometry," Quat. Sci. Rev. **30**(25-26), 3575–3588 (2011).
2. H. Friedli, U. Siegenthaler, D. Rauber, and H. Oeschger, "Measurements of concentration, $^{13}C/^{12}C$ and $^{18}O/^{16}O$ ratios of tropospheric carbon dioxide over Switzerland," Tellus B **39B**(1-2), 80–88 (1987).
3. I. Prokhorov, T. Kluge, and C. Janssen, "Optical clumped isotope thermometry of carbon dioxide," Sci. Rep. **9**(1), 4765 (2019).
4. J. M. McCrea, "On the isotopic chemistry of carbonates and a paleotemperature scale," The J. Chem. Phys. **18**(6), 849–857 (1950).
5. J. Veizer and A. Prokoph, "Temperatures and oxygen isotopic composition of Phanerozoic oceans," Earth-Sci. Rev. **146**, 92–104 (2015).
6. U. Ryb and J. M. Eiler, "Oxygen isotope composition of the Phanerozoic ocean and a possible solution to the dolomite problem," Proc. Natl. Acad. Sci. **115**(26), 6602–6607 (2018).
7. E. L. Grossman, "Applying oxygen isotope paleothermometry in deep time," Paleontol. Soc. Pap. **18**, 39–68 (2012).
8. J. Fiebig, D. Bajnai, N. Löffler, K. Methner, E. Krsnik, A. Mulch, and S. Hofmann, "Combined high-precision Δ_{47} and Δ_{48} analysis of carbonates," Chem. Geol. **522**, 186–191 (2019).
9. D. Bajnai, W. Guo, C. Spötl, T. B. Coplen, K. Methner, N. Löffler, E. Krsnik, E. Gischler, M. Hansen, D. Henkel, G. D. Price, J. Raddatz, D. Scholz, and J. Fiebig, "Dual clumped isotope thermometry resolves kinetic biases in carbonate formation temperatures," Nat. Commun. **11**(1), 4005 (2020).
10. M. Daëron, D. Blamart, M. Peral, and H. P. Affek, "Absolute isotopic abundance ratios and the accuracy of Δ_{47} measurements," Chem. Geol. **442**, 83–96 (2016).
11. Z. Wang, D. D. Nelson, D. L. Dettman, J. B. McManus, J. Quade, K. W. Huntington, A. J. Schauer, and S. Sakai, "Rapid and precise analysis of carbon dioxide clumped isotopic composition by tunable infrared laser differential spectroscopy," Anal. Chem. **92**(2), 2034–2042 (2020).
12. I. Prokhorov, T. Kluge, and C. Janssen, "Laser absorption spectroscopy of rare and doubly substituted carbon dioxide isotopologues," Anal. Chem. **91**(24), 15491–15499 (2019).
13. I. Galli, S. Bartalini, R. Ballerini, M. Barucci, P. Cancio, M. De Pas, G. Giusfredi, D. Mazzotti, N. Akikusa, and P. De Natale, "Spectroscopic detection of radiocarbon dioxide at parts-per-quadrillion sensitivity," Optica **3**(4), 385 (2016).
14. A. J. Fleisher, D. A. Long, Q. Liu, L. Gameson, and J. T. Hodges, "Optical measurement of radiocarbon below unity fraction modern by linear absorption spectroscopy," J. Phys. Chem. Lett. **8**(18), 4550–4556 (2017).
15. Z. Wang, E. A. Schauble, and J. M. Eiler, "Equilibrium thermodynamics of multiply substituted isotopologues of molecular gases," Geochim. Cosmochim. Acta **68**(23), 4779–4797 (2004).
16. X. Cao and Y. Liu, "Theoretical estimation of the equilibrium distribution of clumped isotopes in nature," Geochim. Cosmochim. Acta **77**, 292–303 (2012).
17. I. E. Gordon, L. S. Rothman, R. J. Hargreaves, R. Hashemi, E. V. Karlovets, F. M. Skinner, E. K. Conway, C. Hill, R. V. Kochanov, Y. Tan, P. Wcislo, A. A. Finenko, K. Nelson, P. F. Bernath, M. Birk, V. Boudon, A. Campargue, K.

Optics EXPRESS

V. Chance, A. Coustenis, B. J. Drouin, J.-M. Flaud, R. R. Gamache, J. T. Hodges, D. Jacquemart, E. J. Mlawer, A. V. Nikitin, V. I. Perevalov, M. Rotger, J. Tennyson, G. C. Toon, H. Tran, V. G. Tyuterev, E. M. Adkins, A. Baker, A. Barbe, E. Canè, A. G. Császár, A. Dudaryonok, O. Egorov, A. J. Fleisher, H. Fleurbaey, A. Foltynowicz, T. Furtenbacher, J. J. Harrison, J.-M. Hartmann, V.-M. Horneman, X. Huang, T. Karman, J. Karns, S. Kassi, I. Kleiner, V. Kofman, F. Kwabia-Tchana, N. N. Lavrentieva, T. J. Lee, D. A. Long, A. A. Lukashevskaya, O. M. Lyulin, V. Y. Makhnev, W. Matt, S. T. Massie, M. Melosso, S. N. Mikhailenko, D. Mondelain, H. S. P. Müller, O. V. Naumenko, A. Perrin, O. L. Polyansky, E. Raddaoui, P. L. Raston, Z. D. Reed, M. Rey, C. Richard, R. Tóbiás, I. Sadiek, D. W. Schwenke, E. Starikova, K. Sung, F. Tamassia, S. A. Tashkun, J. Vander Auwera, I. A. Vasilenko, A. A. Vigasin, G. L. Villanueva, B. Vispoel, G. Wagner, A. Yachmenev, and S. N. Yurchenko, "The HITRAN2020 molecular spectroscopic database," J. Quant. Spectrosc. Radiat. Transf. **277**, 107949 (2022).

18. C. Hill, I. E. Gordon, R. V. Kochanov, L. Barrett, J. S. Wilzewski, and L. S. Rothman, "HITRANonline: An online interface and the flexible representation of spectroscopic data in the HITRAN database," J. Quant. Spectrosc. Radiat. Transf. **177**, 4–14 (2016).
19. M. Fischer, B. Tuzson, A. Hugi, R. Brönnimann, A. Kunz, S. Blaser, M. Rochat, O. Landry, A. Müller, and L. Emmenegger, "Intermittent operation of QC-lasers for mid-IR spectroscopy with low heat dissipation: tuning characteristics and driving electronics," Opt. Express **22**(6), 7014 (2014).
20. C. Liu, B. Tuzson, P. Scheidegger, H. Looser, B. Bereiter, M. Graf, M. Hundt, O. Aseev, D. Maas, and L. Emmenegger, "Laser driving and data processing concept for mobile trace gas sensing: Design and implementation," Rev. Sci. Instrum. **89**(6), 065107 (2018).
21. M. Graf, L. Emmenegger, and B. Tuzson, "Compact, circular, and optically stable multipass cell for mobile laser absorption spectroscopy," Opt. Lett. **43**(11), 2434 (2018).
22. M. Graf, P. Scheidegger, A. Kupferschmid, H. Looser, T. Peter, R. Dirksen, L. Emmenegger, and B. Tuzson, "Compact and lightweight mid-infrared laser spectrometer for balloon-borne water vapor measurements in the UTLS," Atmos. Meas. Tech. **14**(2), 1365–1378 (2021).
23. B. Tuzson, M. Graf, J. Ravelid, P. Scheidegger, A. Kupferschmid, H. Looser, R. P. Morales, and L. Emmenegger, "A compact QCL spectrometer for mobile, high-precision methane sensing aboard drones," Atmos. Meas. Tech. **13**(9), 4715–4726 (2020).
24. "Red Pitaya," www.redpitaya.com.
25. B. Tuzson, J. Mohn, M. Zeeman, R. Werner, W. Eugster, M. Zahniser, D. Nelson, J. McManus, and L. Emmenegger, "High precision and continuous field measurements of δ^{13}C and δ^{18}O in carbon dioxide with a cryogen-free QCLAS," Appl. Phys. B **92**(3), 451–458 (2008).
26. E. Moyer, D. Sayres, G. Engel, J. St. Clair, F. Keutsch, N. Allen, J. Kroll, and J. Anderson, "Design considerations in high-sensitivity off-axis integrated cavity output spectroscopy," Appl. Phys. B **92**(3), 467–474 (2008).
27. R. H. Dicke, "The effect of collisions upon the Doppler width of spectral lines," Phys. Rev. **89**(2), 472–473 (1953).
28. S. G. Rautian and I. I. Sobel'man, "The effect of collisions on the Doppler broadening of spectral lines," Sov. Phys. Usp. **9**(5), 701–716 (1967).
29. N. H. Ngo, D. Lisak, H. Tran, and J. M. Hartmann, "An isolated line-shape model to go beyond the Voigt profile in spectroscopic databases and radiative transfer codes," J. Quant. Spectrosc. Radiat. Transf. **129**, 89–100 (2013).
30. J. Cerezo, A. Bastida, A. Requena, and J. Zú niga, "Rovibrational energies, partition functions and equilibrium fractionation of the CO2 isotopologues," J. Quant. Spectrosc. Radiat. Transf. **147**, 233–251 (2014).
31. M. Daëron, R. N. Drysdale, M. Peral, D. Huyghe, D. Blamart, T. B. Coplen, F. Lartaud, and G. Zanchetta, "Most Earth-surface calcites precipitate out of isotopic equilibrium," Nat. Commun. **10**(1), 429 (2019).
32. A. Piasecki, A. Sessions, M. Lawson, A. A. Ferreira, E. V. S. Neto, and J. M. Eiler, "Analysis of the site-specific carbon isotope composition of propane by gas source isotope ratio mass spectrometer," Geochim. Cosmochim. Acta **188**, 58–72 (2016).
33. G. Genoud, J. Lehmuskoski, S. Bell, V. Palonen, M. Oinonen, M.-L. Koskinen-Soivi, and M. Reinikainen, "Laser spectroscopy for monitoring of radiocarbon in atmospheric samples," Anal. Chem. **91**(19), 12315–12320 (2019).
34. P. M. J. Douglas, D. A. Stolper, J. M. Eiler, A. L. Sessions, M. Lawson, Y. Shuai, A. Bishop, O. G. Podlaha, A. A. Ferreira, E. V. Santos Neto, M. Niemann, A. S. Steen, L. Huang, L. Chimiak, D. L. Valentine, J. Fiebig, A. J. Luhmann, W. E. Seyfried, G. Etiope, M. Schoell, W. P. Inskeep, J. J. Moran, and N. Kitchen, "Methane clumped isotopes: Progress and potential for a new isotopic tracer," Org. Geochem. **113**, 262–282 (2017).
35. A. Nataraj, "QCLAS with low temperature multipass cell for clumped thermometry," figshare, 2021, https://doi.org/10.6084/m9.figshare.17197679.v1.